NMR Structures of Two Variants of Bovine Pancreatic Trypsin Inhibitor (BPTI) Reveal Unexpected Influence of Mutations on Protein Structure and Stability

ARTICLE *in* JOURNAL OF MOLECULAR BIOLOGY · SEPTEMBER 2002

Impact Factor: 4.33 · DOI: 10.1016/S0022-2836(02)00620-4 · Source: PubMed

2 AUTHORS, INCLUDING:

Jacek Otlewski
University of Wroclaw
133 PUBLICATIONS **3,694** CITATIONS

SEE PROFILE

doi:10.1016/S0022-2836(02)00620-4 available online at http://www.idealibrary.com on IDEAL® J. Mol. Biol. (2002) 321, 647–658

JMB

NMR Structures of Two Variants of Bovine Pancreatic Trypsin Inhibitor (BPTI) Reveal Unexpected Influence of Mutations on Protein Structure and Stability

Tomasz Cierpicki and Jacek Otlewski*

Laboratory of Protein Engineering, Institute of Biochemistry and Molecular Biology, University of Wroclaw Tamka 2, 50-137 Wroclaw Poland

Here we determined NMR solution structures of two mutants of bovine pancreatic trypsin inhibitor (BPTI) to reveal structural reasons of their decreased thermodynamic stability. A point mutation, A16V, in the solvent-exposed loop destabilizes the protein by 20 °C, in contrast to marginal destabilization observed for G, S, R, L or W mutants. In the second mutant introduction of eight alanine residues at proteinase-contacting sites (residues 11, 13, 17, 18, 19, 34, 37 and 39) provides a protein that denatures at a temperature about 30 °C higher than expected from additive behavior of individual mutations. In order to efficiently determine structures of these variants, we applied a procedure that allows us to share data between regions unaffected by mutation(s). NOAH/DYANA and CNS programs were used for a rapid assignment of NOESY cross-peaks, structure calculations and refinement. The solution structure of the A16V mutant reveals no conformational change within the molecule, but shows close contacts between V16, I18 and G36/G37. Thus, the observed 4.3 kcal/mol decrease of stability results from a strained local conformation of these residues caused by introduction of a β-branched Val side-chain. Contrary to the A16V mutation, introduction of eight alanine residues produces significant conformational changes, manifested in over a 9 Å shift of the Y35 side-chain. This structural rearrangement provides about 6 kcal/mol non-additive stabilization energy, compared to the mutant in which G37 and R39 are not mutated to alanine residues.

Keywords: bovine pancreatic trypsin inhibitor; NMR; stability; solution structure; conformational change

*Corresponding author

Introduction

Analysis of mutations that influence the thermodynamic stability of proteins is of significant practical and theoretical interest. The most often adapted method includes design and purification of a series of mutant proteins, which are subsequently analyzed by thermodynamic and structural methods. The classic examples of this approach comprise extensive studies on T4 lysozyme,[1] barnase,[2] staphylococcal nuclease[3] and T_1 ribonuclease.[4] Combination of thermodynamic and structural data allowed us to determine the specific contributions to protein stability made by a given amino acid residue and also allowed us to understand secondary structure propensity scales,[5,6] packing effects,[7] influence of surface residues[8] and sometimes also the energetics of a single interaction like a hydrogen bond.[9] Nevertheless, there were reported cases showing that rational mutagenesis supported by modeling and/or calculations and subsequently verified by structure determination did not lead to an expected significant increase in overall protein stability.[1] On the contrary, numerous examples show that even a

Abbreviations used: BPTI_A16L, BPTI mutant in which Ala16 is substituted with leucine; BPTI_A16V, BPTI mutant in which Ala16 is substituted with valine; BPTI_G37A, BPTI mutant in which G37 is substituted with Ala; BPTI_WT, wild-type of bovine pancreatic trypsin inhibitor; BPTI_8A, BPTI mutant in which residues T11, P13, A17, I18, I19, V34, G37, A39 are all substituted with alanine; NOE, nuclear Overhauser enhancement; NOESY, NOE spectroscopy; ppm, ppb, parts per million and billion, respectively; T_{den}, denaturation temperature.

E-mail address of the corresponding author: otlewski@bf.uni.wroc.pl

Table 1. Assignment statistics of final NOAH/DYANA calculations

	BPTI_WT	BPTI_A16V	BPTI_8A
Number of peaks	1676 (H_2O $t = 20$ °C)	840 (H_2O $t = 25$°C) 532 (^2H_2O $t = 25$ °C) 553 (H_2O $t = 35$°C)	971 (H_2O $t = 25$ °C)
NOAH assigned peaks	1433 (86%)	725 (86%) 457 (86%) 483 (87%)	812 (84%)
Incompatible peaks	12	2, 1, 5	6
Additional restraints			
ϕ angle restraints	31	–	19
χ1 angle restraints	17	15	9
Hydrogen bonds	24	24	17
Stereo-specific assignment	34	34	20
DYANA target function	0.34 ± 0.059	0.44 ± 0.062	0.27 ± 0.039

single amino acid substitution can lead to unexpected changes in protein stability.[10,11]

Our group has designed, purified and analyzed over 100 mutants of bovine pancreatic trypsin inhibitor (BPTI) with a major aim of determining the energetic role of different contact amino acid residues on the association energy with a number of serine proteinases.[12] We analyzed sets of single mutants comprising P1, P3, P4, P1′ positions of the proteinase binding loop (nomenclature according to Schecter & Berger[13]), variants containing single and multiple alanine substitutions at the proteinase contacting positions[14] and also multiple variants selected from phage display libraries for improved proteinase inhibition.[15] We routinely verified global folding of the mutant proteins by thermodynamic stability parameters. For the majority of BPTI mutants the stability parameters could be rationalized. However, the stability parameters of two variants behaved unexpectedly.

The P1′ mutant A16V BPTI (hereinafter called BPTI_A16V) showed the denaturation temperature lowered by about 20 °C, compared to the wild-type protein (63.8° *versus* 83.6 °C).[16] All remaining five amino acids (G, S, R, L and W) introduced at this position did not lead to the decrease in the stability by more than 3 °C. The X-ray structure of BPTI_A16L in complex with trypsin is very close to the wild-type BPTI[16] and does not explain the large effect caused by the A to V substitution.

The T11A, P13A, R17A, I18A, I19A, V34A, G37A, R39A mutant of BPTI (hereinafter called BPTI_8A) also behaved unusually, as it was more stable than several less extensive mutants, which contained four to six alanine residues.[14] Compared to variant T11A, P13A, R17A, I18A, I19A, V34A ($T_{den} = 48.6$ °C at pH 2.0), BPTI_8A contains two additional mutations: G37A and R39A. Yu *et al.*[17] showed that the former substitution reduced the T_{den} value by 17.2 °C and the latter had no effect on BPTI stability. Thus, following the additivity rule, BPTI_8A should denature at about 31 °C. The measured T_{den} value for BPTI_8A is 60.9 °C.[14] Both BPTI_V16A and BPTI_8A contain two conservative substitutions, K15R and M52L, which do not affect the structure[18] and stability[8] of BPTI. The former mutation was introduced to increase the association constant for interactions with trypsin and chymotrypsin[19] and the latter one to enable CNBr cleavage of a fusion protein during the purification procedure. In order to explain the large effect of the mutations, we decided to investigate its structure using NMR spectroscopy.

Results

Structure determination

In these studies, we determined the structures of BPTI_WT and two variants: BPTI_A16V and BPTI_8A. The main advantage of structure determination of closely related proteins is the possibility to share data between regions unaffected by the mutations. We used chemical shits as a tool to monitor conformational changes and identify unperturbed fragments. Furthermore, amide proton temperature coefficients were applied to compare hydrogen bond network. For rapid NOESY cross-peak assignment and the structure calculation we applied the automatic NOAH routine implemented in the DYANA program.[20]

Structure calculation of the wild-type protein

Structure determination of BPTI was carried out in order to optimize the procedure used for further analysis of BPTI_A16V and BPTI_8A. Manual analysis of proton chemical shifts was followed by automatic assignment of NOESY cross-peaks and structure calculation in the program NOAH/DYANA. Additional data, such as dihedral angle restraints, hydrogen bonds, stereo-specific assignments have been included in order to increase the accuracy of structure calculations. Stereo-specific assignment and $^3J_{HN\alpha}$ coupling constants were taken from the published work.[21] Furthermore, we used the high resolution crystal structure of BPTI_WT (PDB code 5pti) for hydrogen bond identification. Only hydrogen bonds involving amide protons with temperature gradients more positive than −4.6 ppb/K were accepted.[22]

Table 2. Structural statistics of the final CNS refined structures

	BPTI_WT	BPTI_A16V	BPTI_8A
Number of restraints			
Unambiguous distance restrains (all)	1159	890	698
Intraresidual	520	404	344
Sequential	227	180	152
Medium range	127	117	80
Long range	285	189	122
Ambiguous distance restraints[a]	113 (251)	163 (385)	87 (195)
Hydrogen bonds	24	24	17
χ1 angle restraints	17	15	9
$^3J_{HN\alpha}$ coupling constants	46	–	39
Chemical shifts	231	231	217
RMSD from experimental restraints			
Unambiguous distance restraints (Å)	0.0255 ± 0.0007	0.0233 ± 0.0008	0.0212 ± 0.0023
Ambiguous distance restraints (Å)	0.0503 ± 0.0045	0.0075 ± 0.0011	0.0262 ± 0.0063
Hydrogen bond restraints (Å)	0.0326 ± 0.0036	0.0179 ± 0.0032	0.0285 ± 0.0035
Dihedral angle restraints (deg.)	0.2534 ± 0.2308	0.0798 ± 0.0946	1.9993 ± 0.3523
Coupling constants (Hz)	0.898 ± 0.022	–	0.571 ± 0.053
Chemical shifts (ppm)	0.299 ± 0.007	0.283 ± 0.011	0.271 ± 0.008
Deviations from idealized covalent geometry			
Bonds (Å)	0.0038 ± 0.00007	0.0030 ± 0.00009	0.0027 ± 0.00019
Angles (deg.)	0.4969 ± 0.0060	0.4346 ± 0.0122	0.4325 ± 0.0098
Impropers (deg.)	0.3659 ± 0.0125	0.3300 ± 0.0140	0.3191 ± 0.0190
Measures of structure quality			
PROCHECK (Ramachandran plot)			
Residues in most favored regions (%)	74.6	73.7	73.3
Residues in additional allowed regions (%)	25.4	24.8	22.5
Residues in generously allowed regions (%)	–	0.4	3.5
Residues in disallowed regions (%)	–	1.1	0.6
Pairwise RMSD (Å)			
Backbone (N, C^α, C, O)	0.35 ± 0.07	0.69 ± 0.15	1.19 ± 0.29
All heavy atoms	1.12 ± 0.10	1.46 ± 0.16	2.01 ± 0.28

Structure quality was evaluated by PROCHECK program (Laskowski *et al.*).[49] Pairwise RMSD values are calculated between ten conformers for residues 3–56.

[a] Total number of assignment possibilities is shown in parentheses.

Automatic assignment and structure calculations in NOAH/DYANA were followed by the refinement process in the CNS program.[23] Assignment and refinement statistics are presented in Tables 1 and 2, respectively. The final set of ten lowest energy conformers is very close to the X-ray structure. The RMSD value between the set of calculated structures and high resolution BPTI crystal structure for backbone and all heavy atoms of residues 3–56 are 0.77 and 1.43 Å, respectively (Table 3). These results obtained for BPTI_WT allowed us to apply a similar procedure for structure calculations of the two BPTI variants.

Structure determination of the two BPTI mutants

Structure determination of BPTI_A16V and BPTI_8A was achieved in four steps.

Table 3. Comparison of accuracies of calculated BPTI structures using DYANA and CNS

	DYANA		CNS	
	Backbone	Heavy atoms	Backbone	Heavy atoms
BPTI_WT	0.74 ± 0.04[a]	1.43 ± 0.08[a]	0.77 ± 0.04[a]	1.36 ± 0.07[a]
BPTI_A16V	1.16 ± 0.11[b]	1.91 ± 0.09[b]	0.94 ± 0.10[a] 0.95 ± 0.09[b]	1.74 ± 0.09[b]
BPTI_8A	0.82 ± 0.08[c]	1.80 ± 0.10[c]	2.70 ± 1.18[a] 0.58 ± 0.07[c]	1.50 ± 0.12[c]

[a] The ten lowest energy conformers were compared to X-ray BPTI structure (PDB code 5pti). RMSD values (Å) were calculated for residues 3–56.

[b] RMSD values (Å) were calculated for residues 3–14, 17–51, 53–56.

[c] RMSD values (Å) were calculated for residues 3–8, 21–31, 43–51, 53–56.

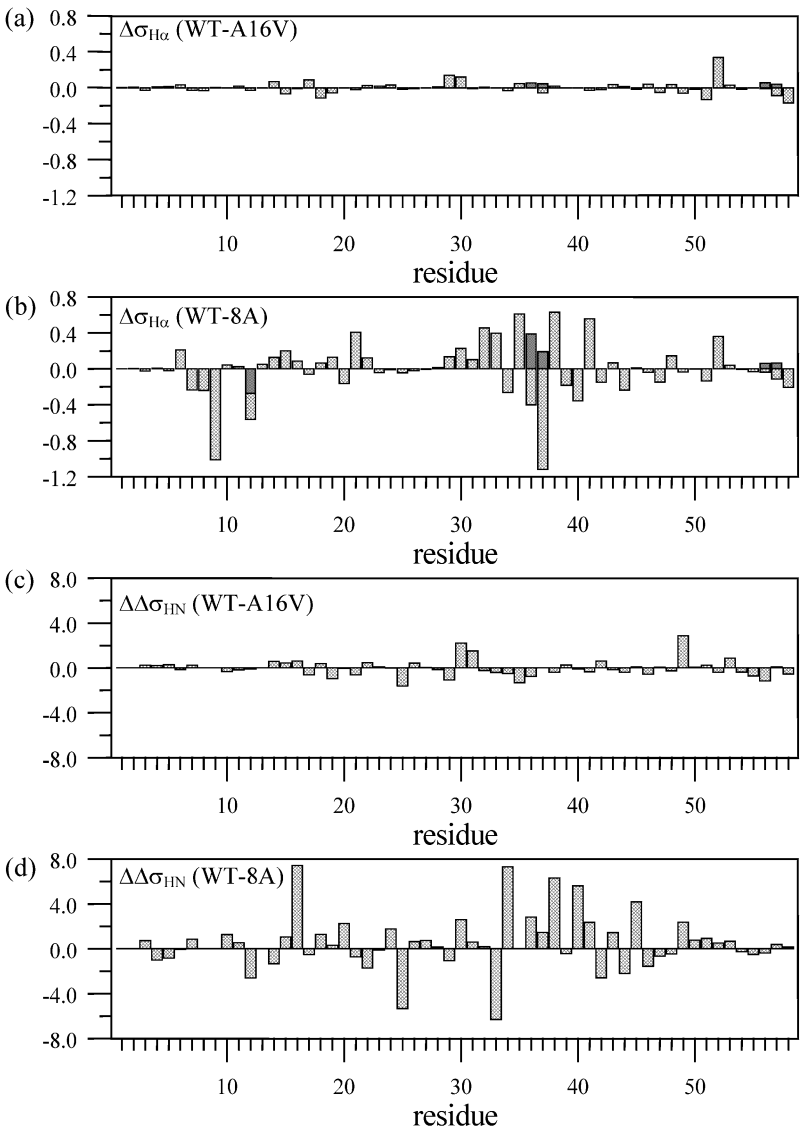

Figure 1. Analysis of chemical shifts and amide proton temperature coefficients for BPTI mutants: chemical shift differences ($\Delta\sigma_{H\alpha}$) between H^{α} atoms of BPTI_WT and BPTI_A16V (a) and BPTI_8A (b); difference between amide proton temperature coefficients ($\Delta\Delta\delta_{HN}/\Delta T$) of BPTI_WT and BPTI_A16V (c) and BPTI_8A (d). Two chemical shift values are shown for Gly residues.

(I) Comparison of chemical shifts between the wild-type protein and each of the mutants and determination of hydrogen bonds and stereo-specific assignments.

(II) Automatic assignment and structure calculation using NOAH/DYANA program.

(III) Identification of additional hydrogen bonds and stereo-specific assignments combined with NOAH/DYANA calculations.

(IV) Refinement in the CNS program.

In the first step, we determined protein fragments sharing unchanged conformations based on the comparison of chemical shifts of the wild-type BPTI and the mutants (see, for example Figure 1). Searching for residues which are not among those replaced in the mutant with no proton chemical shift changes larger than 0.1 ppm compared to BPTI_WT resulted in the following fragments: 1–14, 17–51, 53–58 for BPTI_A16V and 1–8, 21–31, 43–51, 53–58 for BPTI_8A. We applied two criteria to identify hydrogen bonds in BPTI_A16V and BPTI_8A: (i) the amide proton and acceptor atom should exist in non-mutated regions; (ii) the temperature coefficient of amide proton should be more positive than −4.6 ppb/K. Stereo-specific assignments were accepted if chemical shifts were similar to BPTI_WT ($\Delta\sigma < 0.1$ ppm).[24] For residues with stereo-assigned β-methylene protons, corresponding χ1 angle restraints were applied. Homology-derived data used for NOAH/DYANA calculations are presented in Table 4.

Second step of structure determination involved automatic assignment and structure calculation in the NOAH/DYANA program. The applied procedure was similar to our previously described work.[25] The first round of NOAH/DYANA was performed in order to check and modify the peak lists used for further analysis. Manual inspection of NOESY spectra allowed us to remove some incompatible peaks with no assignment possibility (noise peaks or peaks arising from interactions with water).[26] The second round of NOAH/DYANA calculations was run using modified peak lists.

Table 4. Stereo-specific assignment and hydrogen bond restraints used during NOAH/DYANA calculations

	BPTI_WT	BPTI_A16V	BPTI_8A
Stereo-specific assignment (adapted from Berndt *et al.*[21])[a]	H^{α}: 12, 28, 37 H^{β}: 2, 4, 8, 9, 14, 15, 17, 20, 22–24, 30, 31, 33, 35, 41–43, 45, 47, 51, 52 H^{γ}: 2, 9 CH^{γ}_3: 34 H^{δ}: 2, 9 $H^{\delta 2}$: 24, 43, 44 CH^{δ}_3: 6	H^{α}: 12, 28, 37 H^{β}: 2, 4, 8, 9, 14, 20–24, 30, 31, 33, 35, 41–43, 45, 47, 51 H^{γ}: 2, 9 CH^{γ}_3: 34 H^{δ}: 2, 9 $H^{\delta 2}$: 24, 43, 44 CH^{δ}_3: 6	H^{α}: 28 H^{β}: 2, 4, 22–24, 30, 43, 45, 47, 51 H^{γ}: 2 H^{δ}: 2 $H^{\delta 2}$: 24 CH^{δ}_3: 6
Stereo-specific assignment according to GLOMSA[b]		CH^{γ}_3: 16 CH^{δ}_3: 29	H^{α}: 36 H^{β}: 9, 20, 33 CH^{δ}_3: 52
Hydrogen bonds[c]	$5H^N$–2O; $6H^N$–3O; $7H^N$–4O; $18H^N$–35O; $20H^N$–33O; $21H^N$–45O; $22H^N$–31O; $23H^N$–$43O^{\delta 1}$; $24H^N$–29O; $26H^N$–$24O^{\delta 1}$; $27H^N$–$24O^{\delta 1}$; $28H^N$–24O; $31H^N$–22O; $33H^N$–20O; $35H^N$–18O; $36H^N$–11O; $43H^N$–$7O^{\varepsilon 1}$; $44H^N$–42O; $45H^N$–21O; $51H^N$–47O; $52H^N$–48O; $53H^N$–49O; $54H^N$–50O; $56H^N$–52O	$5H^N$–2O; $6H^N$–3O; $7H^N$–4O; $18H^N$–35O; $20H^N$–33O; $21H^N$–45O; $22H^N$–31O; $23H^N$–$43O^{\delta 1}$; $24H^N$–29O; $26H^N$–$24O^{\delta 1}$; $27H^N$–$24O^{\delta 1}$; $28H^N$–24O; $31H^N$–22O; $33H^N$–20O; $35H^N$–18O; $36H^N$–11O; $43H^N$–$7O^{\varepsilon 1}$; $44H^N$–42O; $45H^N$–21O; $51H^N$–47O; $52H^N$–48O; $53H^N$–49O; $54H^N$–50O; $56H^N$–52O	$5H^N$–2O; $6H^N$–3O; $7H^N$–4O; $21H^N$–45O; $22H^N$–31O; $23H^N$–43OD1; $24H^N$–29O; $26H^N$–$24O^{\delta 1}$; $27H^N$–$24O^{\delta 1}$; $28H^N$–24O; $31H^N$–22O; $51H^N$–47O; $52H^N$–48O; $53H^N$–49O; $54H^N$–50O; $56H^N$–52O
Additional hydrogen bonds			$37H^N$–34O

[a] Stereospecifically assigned atoms are followed by amino acid positions.
[b] Stereospecific assignments obtained from GLOMSA program (Guntert *et al.*)[27] were based on preliminary calculated structures.
[c] Donor and acceptor atoms are shown for hydrogen bonds.

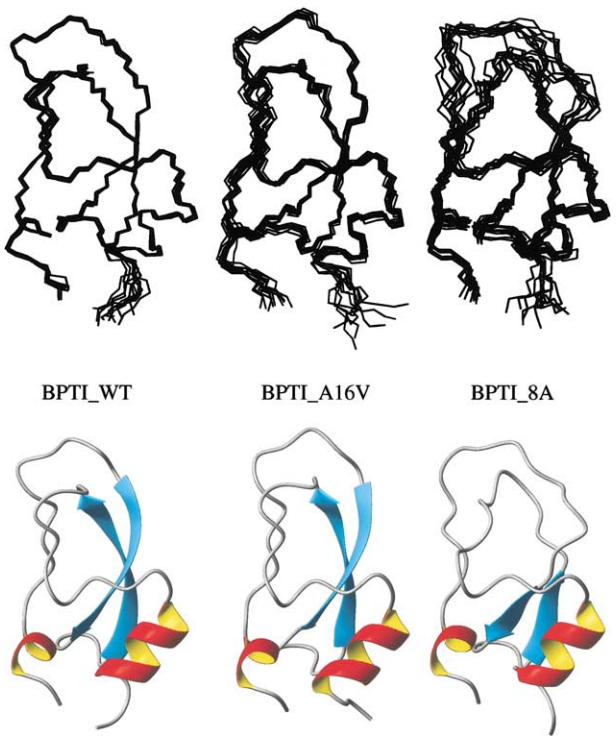

Figure 2. Comparison of calculated structures of BPTI_WT, BPTI_A16V and BPTI_8A. Upper pictures show the backbones of the ten lowest energy structures and lower pictures show their ribbon representation.

Step (III) included analysis of calculated structures and a search for additional stereo-specific assignment using the GLOMSA program.[27] Furthermore, we identified one additional hydrogen bond for BPTI_8A based on geometrical criteria and the low temperature gradient of the A37 amide proton. All collected data (see Table 4) were applied in NOAH/DYANA calculations starting from unassigned peak lists.[25] This step was repeated twice and final assignment statistics are presented in Table 1.

We applied the final step (IV) to refine structures in program CNS using NOAH assigned distance restraints, hydrogen bonds, dihedral angle restraints, $^3J_{HN\alpha}$ coupling constants and proton chemical shifts. Furthermore, we applied ambiguous restraints for unassigned peaks with more than one assignment possibility.[28] Calculated structures of BPTI_WT, BPTI_A16V and BPTI_8A are compared in Figures 2 and 3 and final refinement statistics are shown in Table 2. The lower precision of BPTI_A16V relative to BPTI_WT results from a smaller number of restraints.

Structure of BPTI_A16V

Structural changes resulting from a single amino acid substitution in a protein may be easily identified comparing their chemical shifts, and one of the most sensitive nuclei to ϕ/ψ angles is H^{α}.[29] Comparison of conformational shifts of H^{α} protons, $\Delta\sigma_{H\alpha}$ of BPTI_A16V and BPTI_WT revealed only small variations, usually not exceeding 0.1 ppm (Figure 1(a)). Furthermore, no noticeable

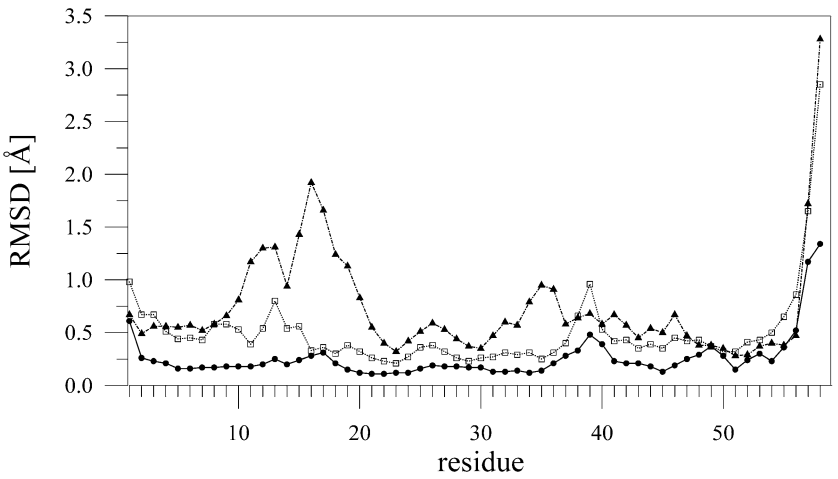

Figure 3. Comparison of local RMDS values for backbone atoms of BPTI_WT (—●—), BPTI_A16V (···□···), BPTI_8A (·–·▲·–·) and their mean structures. The less precisely defined structure of BPTI_A16V relative to BPTI_WT results from a smaller number of experimental restraints. Fragment 9–20 of BPTI_8A is poorly defined.

differences between side-chain proton chemical shifts of the two proteins were found (data not shown). The largest observed difference in $\Delta\sigma_{H\alpha}$ results from the conservative M52L substitution. Small residual variations may result from differences in the experimental conditions, such as pH. Very similar conformational shifts of H^{α} within the region 13–17 suggest that the A16V substitution does not alter the binding loop structure.

Comparison of temperature coefficients of amide protons further confirms the lack of structural changes in the mutant (Figure 1(c)). Very similar profiles of $\Delta\sigma_{HN}/\Delta T$provide evidence for preservation of hydrogen bond network. The largest difference is observed for E49. However, this was reported previously and results from a different pH value.[22] The amide proton of E49 forms a hydrogen bond with its side-chain carboxyl group at pH 4.6, while this hydrogen bond is lost at pH 3 leading to a more negative value of $\Delta\sigma_{HN}/\Delta T$.

The solution structure of BPTI_A16V is consistent with the analysis of chemical shifts and $\Delta\sigma_{HN}/\Delta T$. The RMSD value between a set of calculated BPTI_A16V structures and BPTI_WT for backbone atoms of residues 3–56 is 0.94 Å (Table 3). This value is close to that obtained from comparison of the BPTI_WT solution structure reported here and the BPTI crystal structure deposited under code 5pti (Table 3) and approaches the accuracy of our calculations. A detailed comparison of BPTI_A16V and the crystal structure of BPTI_WT shows no detectable differences within the region of the P1′ mutation (Figure 4). The C^{β} atoms of A16 and V16 occupy similar positions in the structure. The presence of several NOEs involving H^{α} of G37 and side-chains of V16 and I18 (G37 $H^{\alpha 2}$-V16 $CH_3^{\gamma 2}$; G37 $H^{\alpha 2}$-V16 $CH_3^{\delta 2}$; G37 $H^{\alpha 1}$-I18 $CH_3^{\delta 1}$; G37 $H^{\alpha 2}$-I18 $CH_3^{\delta 1}$) additionally confirms the accuracy of the calculated BPTI_A16V structure. As mentioned above, the A16L mutation does not affect the thermodynamic stability of BPTI. The crystal structure of the P1′ Leu variant of BPTI (BPTI_A16L) in complex with trypsin reveals a different conformation of I18 (Figure 4(a)), which results probably from the enzyme–inhibitor interaction and competition between P1′ (L16) and P3′ (I18) for the same binding site in trypsin.[16] Thus, the structure of BPTI_A16L does not explain the destabilizing effect caused by the A16V substitution. Furthermore, the significant change in stability does not correspond to any noticeable differences in the structure of BPTI_A16V compared to BPTI_WT.

Very recently the structure of BPTI_G37A was determined by NMR spectroscopy.[24] At pH 2.0, the G37A mutation destabilizes protein by 4.9 kcal/mol[30] which is comparable to loss of 4.3 kcal/mol upon A16V substitution.[16] Furthermore, BPTI_G37A similarly shows almost no structural changes compared to BPTI_WT. The key residue responsible for the observed effect is G37,

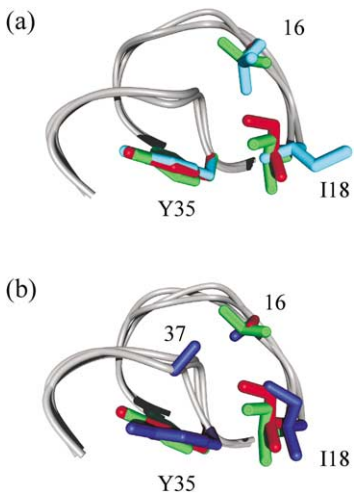

Figure 4. Comparison of binding loop conformations (residues 11–18 and 34–40) of various BPTI mutants: BPTI_WT (PDB code 5pti), red; BPTI_A16V , green; BPTI_A16L (PDB code 1ejm), cyan; BPTI_G37A, blue. (a) Comparison of the effects of A16V and A16L mutations; (b) comparison of A16V and G37A mutations. For the reason of clarity only single conformers of the NMR structures are displayed.The Figure was prepared in MOLMOL/POV-Ray.

which is involved in an unusual H^N-aromatic–$H^{\delta 22}$ interaction network between its backbone amide, the aromatic ring of Y35 and the N44 side-chain amide proton. Glycine is the only residue capable of the ϕ and ψ dihedral angles required for this interaction. Thus, the addition of just one methyl group in BPTI_G37A results in a locally strained backbone conformation. Interestingly, mutation of A16V leads to a very similar effect, but in this case the strain is caused by methyl group of V16. Superposition of the crystal structures of BPTI_WT, BPTI_A16V and BPTI_G37A shows that the $\gamma 2$ methyl group of V16 may have a similar effect as methyl group of A37, affecting the backbone conformation of G36 and G37 (Figure 4(b)). While disallowed dihedral angles of A37 result from steric hindrance between side-chain methyl and main-chain carbonyl groups, the side-chain of V16 interferes with backbone atoms of G36 and G37. Furthermore, preservation of amide-aromatic interactions in BPTI_A16V is manifested in the lack of chemical shifts changes of the two amides G37 H^N (4.32 and 4.26 ppm for BPTI_WT and BPTI_A16V, respectively) and N44 $H^{\delta 22}$ (3.39 and 3.41 ppm for BPTI_WT and BPTI_A16V, respectively).

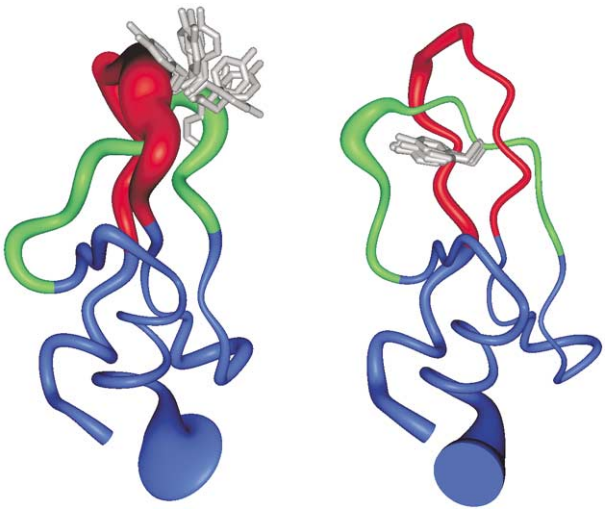

Figure 5. "Sausage" representation of BPTI_8A (left) and BPTI_A16V (right) created based on a set of ten structures with a line radius proportional to local the RMSD. Structurally conserved fragments of the two mutants (shown in blue) are oriented in the same way. Rearrangement of 32–42 loop (green) in BPTI_8A compared to BPTI_A16V is accompanied by a significant change of the position of Y35 (gray). The second loop, comprising residues 9–20 (shown in red) and containing the proteinase binding site, is much less ordered in BPTI_8A than in BPTI_A16V and BPTI_WT.

Structure of BPTI_8A

Comparison of H^α secondary shifts between BPTI_WT and BPTI_8A shows large differences, indicating substantial conformational changes (Figure 1(b)). The largest differences in chemical shift are observed for both backbone and side-chain protons within the 32–42 fragment. Furthermore, considerable changes of amide proton temperature coefficients also indicate an alteration of the hydrogen bond pattern (Figure 1(d)).

The NMR structure of BPTI_8A confirms the presence of significant changes induced by mutations of eight amino acid residues to alanine. Structurally conserved fragments consist of residues 3–8, 21–31 and 43–56 and comprise the core of BPTI. Large conformational change occurs in fragment 32–42 while the binding loop residues (9–20) are poorly defined (Figure 3). The most spectacular structural change in the mutant involves the Y35 residue that is expelled outside the protein core and exposed to solvent (Figure 5). The side-chain of Y35 moves away by more than 9 Å (comparing distance between C^β atoms of Y35 in BPTI_WT and BPTI_8A). Loss of characteristic amide–aromatic interactions involving ring of Y35, A37 H^N and N44 $H^{\delta 22}$ is manifested in significant chemical shift changes of the amide groups. The amide proton of residue 37 is shifted downfield by 3.43 ppm (4.32 and 7.75 ppm for G37 and A37 in BPTI_WT and BPTI_8A, respectively) and chemical shifts of side-chain amide protons of N44 ($H^{\delta 21}$ and $H^{\delta 22}$) are changed from 3.41 and 7.86 ppm in BPTI_WT to 6.61 and 7.23 ppm in BPTI_8A. This structural rearrangement is accompanied by shortening of the central β-sheet and loosening of its three hydrogen bonds (18 H^N–35 O; 20 H^N–33 O; 35 H^N–18 O). The most probable reason for the change is related to the loss of hydrophobic interactions of three truncated side-chains (I18A, I19A, V34A). Such unfavorable rearrangement is partially compensated by formation of a type II β-turn comprising residues 34–37 and the 37 H^N–34 O hydrogen bond. Further stabilization of BPTI_8A may involve formation of a short antiparallel β-sheet, comprising residues 10, 11 and 37, 38. However, only a few weak interstrand NOEs are observed for this region (10 H^N–38 H^N; 11 H^α–38 H^N; 12 H^N–37 H^α and NOEs between side-chains of Tyr10 and Cys38) and it is difficult to prove unambiguously the existence of this β-structure. Small side-chains of adjacent Ala11 and A37 do not provide stabilizing interstrand hydrophobic interactions. Furthermore, temperature coefficients of amide protons of Y10 and C38 (−7.1 and −7.6 ppb/K, respectively) do not confirm the presence of interstrand hydrogen bonds.

The binding loop-containing region (residues 9–20) composed mainly of Ala residues is poorly structured. Two reasons might be responsible for this observation: lack of larger side-chains does not provide either electrostatics or hydrophobic interactions and the limited number of long-range NOEs does not allow us to precisely define the structure in this area. However, considerable inhibitory activity of BPTI_8A, especially against chymotrypsin, proves that the canonical conformation of the binding loop should be retained and

enable interactions with trypsin and chymotrypsin.[14]

Discussion

Here, we point out the advantages arising from structure determination of closely related proteins. The most evident feature of the mutant analysis results from the conservation of chemical shifts, which speeds up assignment significantly. Furthermore, comparison of chemical shifts and amide proton temperature coefficients might be used to identify structurally conserved fragments. For such regions, additional data, such as hydrogen bonds and stereo-specific assignments, may be shared during structure calculation. Application of automatic methods for assignment of NOESY cross-peaks and structure calculation should significantly reduce the time required for structure determination.

Application of amide proton temperature coefficients

Temperature coefficients of H^N protons carry valuable information on the hydrogen bonding status of amide protons.[22] Additionally, they may be very useful in analysis of related proteins providing information about conservation of hydrogen bonding patterns. Lack of structural changes upon the A16V mutation is reflected in preservation of $\Delta\sigma_{HN}/\Delta T$ values (Figure 1). The large conformational transition observed for BPTI_8A is accompanied by substantial changes of hydrogen bonding network and is manifested in large changes of $\Delta\sigma_{HN}/\Delta T$ values (Figure 1). Thus, amide proton temperature gradients together with chemical shifts may determine the criteria used to accept hydrogen bonds in structure calculations of a series of mutants.

Values of $\Delta\sigma_{HN}/\Delta T$correlate very well with the presence of hydrogen bonds for conserved part of BPTI. However, a few anomalous temperature coefficients are observed for amide protons residing in the rearranged region of BPTI_8A. The positive gradient $\Delta\sigma_{HN}/\Delta T = 4.0$ ppb/K for H^N F33, the large negative gradient $\Delta\sigma_{HN}/\Delta T = -14.8$ ppb/K for H^N A34 and lack of an amide proton of Y35 may indicate the conformational exchange in this region. Furthermore, the temperature gradient of the hydrogen bonded amide proton of F45 exhibits a large difference between BPTI_WT and BPTI_8A: −3.4 and −7.6 ppb/K, respectively. A few interstrand NOEs found between residues 10, 11 and 37, 38 suggest the presence of a short antiparallel β-sheet. However, temperature coefficients of amide protons of Y10 and C38 (−7.1 and −7.6 ppb/K, respectively) do not confirm formation of interstrand hydrogen bonds. Anomalous temperature gradients are often observed for peptides and correspond to a decrease in population of the structured state upon heating.[31] Loss of numerous tertiary contacts due to substitution of eight residues into alanine might result in a less stable region which is anchored on the unchanged, rigid core of BPTI.

BPTI_A16V

Substitution of the partially exposed residue A16 with valine led to a significant, about 20 °C, decrease in denaturation temperature, equivalent to a 4.3 kcal/mol decrease in the free energy of stabilization.[17] Thus, substitution of a single residue at the partially exposed position in the proteinase binding loop is responsible for the similar effect to some crevice forming mutations in the protein core.[30] However, this mutation is not accompanied by any structural changes or loss of electrostatic or hydrophobic interactions. Our previous study of amino acid substitutions at the fully exposed P1 site of BPTI showed about 11 degrees difference in the ΔT_{den} value between the least (P1 Trp) and most (P1 His) stable variant.[8] A correlation analysis with different properties of amino acids suggested that the two mechanisms might be responsible for the observed differences at P1 site: the reverse hydrophobic effect and amino acid propensities to occur in non-optimal dihedral angles adopted by the P1 position. In contrast to the P1 site, the residue in the P1′ position is in the extended conformation ($\phi = -76°$ and $\psi = 168°$) which is very favorable for the β-branched Val side-chain. Furthermore, the hydrophobic effect can be excluded because the A16L substitution leads to an even slightly more stable mutant ($\Delta\Delta G = 0.6$ kcal/mol).[16]

The observed effect is comparable to the recently described structure of BPTI_G37A.[24] Lack of any significant differences in chemical shifts upon G37A substitution confirms the absence of structural changes. Many residues in the region of the mutation, however, show increased flexibility compared to BPTI_WT. Although no additional experiments confirming altered dynamics in BPTI_A16V were carried out, chemical shift analysis is more consistent with BPTI_G37A. A smaller dispersion of chemical shifts of Y35 aromatic protons compared at the same temperatures (data not shown) is consistent with a lower rotational barrier for BPTI_A16V compared to BPTI_WT.

It appears that the significant decrease in BPTI_A16V stability arises from the strain between the side-chains of V16, I18 and the backbone of G37. This is confirmed in sizeable intensities of NOEs between H^α protons of G37 and the δ1 methyl group of I18. The importance of proper conformation of G36 and G37 in terms of interaction with Y35 and stabilization of protein structure has been described.[24] It is, however, very interesting that a comparable effect may be caused by local strain due to energetically unfavorable ϕ, ψ angles of A37 as well as a result from addition of a methyl group coming from a residue close in space. The presence of the β-branched residue at

position 16, which is adjacent to residues 36 and 37, does not allow for relaxation of the local structure without changes in backbone conformation. This leads to a strain and results in decreasing the thermodynamic stability. Furthermore, the A16V mutation is likely to increase the local dynamics relative to BPTI_WT. Such an effect is not observed when non-β-branched side-chains such as that of L, R or W are present at position 16.

BPTI_8A

Previous studies showed that the BPTI fold may accepts almost 50% of alanine residues without disturbing its overall structure.[32] It was also shown that the denaturation temperature of mutants containing up to 27 alanine residues could be predicted by the sum of the change in denaturation temperature for single mutants.[32] This is in agreement with the additivity effect commonly observed in protein–protein interactions, enzyme catalysis and protein stability.[33] However, Kuroda & Kim[32] mutated into alanine residues only those showing little impact on protein stability, while the hydrophobic core was preserved. On the other hand, probing the structural epitope of BPTI responsible for proteinase binding by alanine having required to modify the residues important for stabilization of the protein tertiary structure such as I18, I19, V34.[14] Nevertheless, additivity cycle analysis showed that all BPTI variants with up to six residues substituted with alanine (including residues 18, 19 and 34) resulted in perfectly additive decreases of thermodynamics stability. Following the additivity rule, BPTI_8A should be only marginally stable at pH 2.0 with the T_{den} value slightly above 30 °C, since the T11A, P13A, R17A, I18A, I19A, V34A variant denatures at 48.6 °C[14] and two additional mutations, G37A and R39A, further reduce T_{den} by 17.2 °C.[17] Instead, the experimentally determined T_{den} value for BPTI_8A is about 30 °C higher,[14] equivalent to about 6 kcal/mol of non-additive free energy of stabilization.

Mutation of eight residues into alanine resulted in the substantial rearrangement of BPTI structure and unexpected gain in thermodynamics stability. Loss of stabilizing interactions is partially compensated but this is not sufficient to maintain a rigid backbone conformation. The perturbed part of BPTI is less precisely defined, as it shows a higher RMSD value relative to the rest of the molecule. This is further confirmed in anomalous values of a few amide proton temperature coefficients and lack of H^N Y35. The structure of BPTI_8A emphasizes the role of the Y35 residue in maintaining rigidity of two loops in BPTI. A single mutation of Y35G leads to a decrease in protein stability by 5 kcal/mol and causes a large conformational exchange on a microsecond time scale[34] for residues that are substituted in BPTI_8A.

The biological activity of protein inhibitors results from the presence of a binding loop, which is highly complementary in shape to the enzyme's active site.[35,36] The binding loop is a solvent-exposed fragment anchored to protein scaffold and its conformation is further stabilized by local side-chain interactions.[37] Structural analysis of BPTI_8A provides some intriguing features concerning the binding loop in this protein. The sequence of the binding loop 11–19 segment of BPTI_8A AGACRAAAA is composed mainly of alanine residues. The side-chain of R15 is solvent-exposed and only a disulfide bridge between Cys14 and Cys38 provides stabilizing interactions. In consequence, this region is significantly less structured compared to the wild-type protein. Although poorly structured, the binding loop possesses the ability to adopt a proper conformation and interacts with trypsin and chymotrypsin. Both enzymes, after prolonged incubation with BPTI_8Ala at pH 8.3, can cleave peptide bond(s) within this segment, as deduced from the loss of inhibitory activity.[14]

In conclusion, solution structures of two BPTI variants, BPTI_A16V and BPTI_8A, provide information on an unexpected influence of mutation(s) on protein structure and stability. Lack of structural changes observed for BPTI_A16V and substantial rearrangement of the BPTI_8A structure result in a similar drop in the thermodynamic stability. Such effects are difficult to predict based on the wild-type protein structure and should be considered in protein engineering.

Materials and Methods

Sample preparation

BPTI_WT (Traskolan) was a generous gift from Jelfa Pharmaceutical Company S.A. (Poland). A 15 mM sample of BPTI_WT at pH 4.6 was prepared for NMR spectroscopy. Mutagenesis, overexpression and purification of BPTI mutants have been described.[14,16] Measurements were carried out for 4 mM (pH 3.1) and 3 mM (pH 2.9) samples of BPTI_A16V and BPTI_8A, respectively.

NMR spectroscopy

All two-dimensional NMR spectra were measured on a Varian Unity Plus 500 and Bruker DRX 500 spectrometers. TOCSY spectra[38] with MLEV-17 spin lock[39] and mixing time 80 ms, DQF-COSY[40] and NOESY spectra[41] with mixing times of 150 ms were recorded in H_2O and ^2H_2O solutions. Spectra were typically collected as 4096 and 512 complex points and data processing was performed with the NMRPipe program.[42] Time domain data were multiplied with a cosine bell window function in both dimensions, followed by zero filling to 2048 points in t_1. In all two-dimensional spectra recorded in H_2O solution, the water signal was suppressed using the WET method[43] or pre-saturation. Temperature dependence of chemical shifts was analyzed from a set of NOESY spectra recorded between 15 and 35 °C.

Analysis of NMR spectra

Chemical shifts were assigned applying a combination of TOCSY/NOESY techniques.[44] Our assignment is in a very good agreement with previously published data.[21] Essentially complete assignments were obtained for the two BPTI mutants. Amide proton temperature coefficients for BPTI_WT were derived from previous work.[45] Values of $\Delta\sigma_{HN}/\Delta T$ for the mutants were calculated as a best fit to chemical shifts measured at different temperatures. Integration and peak picking of NOESY spectra were carried out in the program Sparky,[46] applying a manual procedure.

Dihedral angle, stereo-specific assignment and hydrogen bond analysis

Stereo-specific assignment and $^3J_{HNH\alpha}$ coupling constants for BPTI_WT were derived from previously published data.[21] For stereo-specifically assigned β-methylene groups corresponding χ1 dihedral angle restraints were added (±45° from ideal rotamer angles). Two broad ranges were used for φ dihedral angles: $-10° \leq \phi \leq -90°$, when $^3J_{HNH\alpha} \leq 5$ Hz and $-80° \leq \phi \leq -175°$ for $^3J_{HNH\alpha} \geq 8$ Hz. Hydrogen bond restraints for BPTI_WT were applied according to two criteria: (i) a hydrogen bond should be present in the BPTI X-ray structure; and (ii) temperature coefficients of the amide proton chemical shifts should be more positive than −4.6 ppb/K.[22] All collected non-NOE based restraints were used for the NOAH/DYANA calculation of BPTI_WT. Some of the non-NOE based restraints were also applied during calculation of the mutant structures. At the beginning, a chemical shift comparison for conserved regions of BPTI mutants was used to identify fragments with unperturbed conformation. For such analysis, chemical shifts of non-exchangeable protons with a chemical shift difference (relative to BPTI_WT) smaller than 0.1 ppm were used. Fragments 1–14, 17–51, 53–58 of BPTI_A16V and 1–8, 21–31, 43–51, 53–58 of BPTI_8A, respectively, were found to be structurally conserved with respect to BPTI_WT. Finally, this analysis served to identification of stereo-specific assignment and χ1 angle restraints for the mutants. Additional stereo-specific assignments were obtained using GLOMSA based on preliminary calculated structures. Hydrogen bonds were used if the amide proton temperature coefficients were more positive than −4.6 ppb/K. One new hydrogen bond between G37 H^N and A34 O in BPTI_8A was identified (a small temperature gradient and consistent appearance within calculated conformers) and used during NOAH/DYANA calculations. Restraints for φ dihedral angles were assigned from $^3J_{HNH\alpha}$ coupling constants (as described above) measured from DQF-COSY using the ACME program.[47]

Structure calculation

The program NOAH/DYANA,[48] with standard parameters, was applied for automatic assignment of NOESY derived cross-peaks applying a previously described procedure.[25] Tolerance ranges used for the assignment differed slightly, depending on data quality, and were 0.012, 0.012, 0.013 ppm for BPTI_WT, BPTI_A16V and BPTI_8A, respectively. Cross-peaks were automatically assigned during several rounds of NOAH/DYANA calculations. Structures of all proteins were refined in the program CNS[23] applying the simulated annealing protocol and using NOE-based distance restraints, hydrogen bonds, proton chemical shifts and dihedral angle restraints. For cross-peaks not assigned by NOAH/DYANA ambiguous distance restraints were created and used during CNS refinement.[28] Structure quality was analyzed using the PROCHECK program.[49] Figures were prepared in the MOLMOL program.[50,51]

Protein Data Bank accession numbers

The coordinates of an ensamble of lowest energy structures have been deposited in the RSCB PDB (accession codes 1ld5 and 1ld6 for BPTI_A16V and BPTI_8A, respectively).

Acknowledgments

We thank Professor Andrzej Ejchart for the use of the NMR spectrometer and Dr Igor Zhukov for assistance in setting up NMR experiments. This work was supported by grant 6PO4A 02119 from the Polish Committee for Scientific Research. T.C. was supported by a young scientist fellowship from the Foundation for Polish Science. J.O. is a Scholar of the Foundation for Polish Science. Calculations were carried out using hardware resources of the Supercomputing and Networking Centre in Wrocław (WCSS).

References

1. Matthews, B. W. (1995). Studies on protein stability with T4 lysozyme. *Advan. Protein Chem.* **46**, 249–278.
2. Fersht, A. R. (1993). The sixth Datta lecture. Protein folding and stability: the pathway of folding of barnase. *FEBS Letters*, **325**, 5–16.
3. Shortle, D. (1995). Staphylococcal nuclease: a showcase of *m*-value effects. *Advan. Protein Chem.* **46**, 217–247.
4. Pace, C. N., Shirley, B. A., McNutt, M. & Gajiwala, K. (1996). Forces contributing to the conformational stability of proteins. *FASEB J.* **10**, 75–83.
5. Blaber, M., Zhang, X. J. & Matthews, B. W. (1993). Structural basis of amino acid alpha helix propensity. *Science*, **260**, 1637–1640.
6. Minor, D. L., Jr & Kim, P. S. (1994). Measurement of the beta-sheet-forming propensities of amino acids. *Nature*, **367**, 660–663.
7. Chen, J. & Stites, W. E. (2001). Packing is a key selection factor in the evolution of protein hydrophobic cores. *Biochemistry*, **40**, 15280–15289.
8. Krowarsch, D. & Otlewski, J. (2001). Amino-acid substitutions at the fully exposed P1 site of bovine pancreatic trypsin inhibitor affect its stability. *Protein Sci.* **10**, 715–724.
9. Pace, C. N., Horn, G., Hebert, E. J., Bechert, J., Shaw, K., Urbanikova, L. *et al.* (2001). Tyrosine hydrogen bonds make a large contribution to protein stability. *J. Mol. Biol.* **312**, 393–404.
10. Mok, Y. K., Elisseeva, E. L., Davidson, A. R. & Forman-Kay, J. D. (2001). Dramatic stabilization of an SH3 domain by a single substitution: roles of the folded and unfolded states. *J. Mol. Biol.* **307**, 913–928.
11. Robinson, C. R. & Sauer, R. T. (2000). Striking stabilization of Arc repressor by an engineered disulfide bond. *Biochemistry*, **39**, 12494–12502.

12. Otlewski, J., Jaskólski, M., Buczek, O., Cierpicki, T., Czapinska, H., Krowarsch, D. *et al.* (2001). Structure–function relationship of serine protease–protein inhibitor interaction. *Acta Biochim. Pol.* **48**, 419–428.
13. Schechter, P. & Berger, A. (1967). On the size of the active site in proteases. I. Papain. *Biochem. Biophys. Res. Commun.* **27**, 157–162.
14. Buczek, O., Koscielska-Kasprzak, K., Krowarsch, D., Dadlez, M. & Otlewski, J. (2002). Analysis of serine proteinase–inhibitor interaction by alanine shaving. *Protein Sci.* **11**, 806–819.
15. Kiczak, L., Kasztura, M., Koscielska-Kasprzak, K., Dadlez, M. & Otlewski, J. (2001). Selection of potent chymotrypsin and elastase inhibitors from M13 phage library of basic pancreatic trypsin inhibitor (BPTI). *Biochim. Biophys. Acta*, **1550**, 153–163.
16. Grzesiak, A., Helland, R., Smalas, A. O., Krowarsch, D., Dadlez, M. & Otlewski, J. (2000). Substitutions at the P(1) position in BPTI strongly affect the association energy with serine proteinases. *J. Mol. Biol.* **301**, 205–217.
17. Yu, M. H., Weissman, J. S. & Kim, P. S. (1995). Contribution of individual side-chains to the stability of BPTI examined by alanine-scanning mutagenesis. *J. Mol. Biol.* **249**, 388–397.
18. Czapinska, H., Otlewski, J., Krzywda, S., Sheldrick, G. M. & Jaskolski, M. (2000). High-resolution structure of bovine pancreatic trypsin inhibitor with altered binding loop sequence. *J. Mol. Biol.* **295**, 1237–1249.
19. Krowarsch, D., Dadlez, M., Buczek, O., Krokoszynska, I., Smalas, A. O. & Otlewski, J. (1999). Interscaffolding additivity: binding of P1 variants of bovine pancreatic trypsin inhibitor to four serine proteases. *J. Mol. Biol.* **289**, 175–186.
20. Mumenthaler, C., Güntert, P., Braun, W. & Wüthrich, K. (1997). Automated combined assignment of NOESY spectra and three-dimensional protein structure determination. *J. Biomol. NMR*, **10**, 351–362.
21. Berndt, K. D., Güntert, P., Orbons, L. P. & Wüthrich, K. (1992). Determination of a high-quality nuclear magnetic resonance solution structure of the bovine pancreatic trypsin inhibitor and comparison with three crystal structures. *J. Mol. Biol.* **227**, 757–775.
22. Cierpicki, T. & Otlewski, J. (2001). Amide proton temperature coefficients as hydrogen bond indicators in proteins. *J. Biomol. NMR*, **21**, 249–261.
23. Brunger, A. T., Adams, P. D., Clore, G. M., DeLano, W. L., Gros, P., Grosse-Kunstleve, R. W. *et al.* (1998). Crystallography & NMR system: a new software suite for macromolecular structure determination. *Acta Crystallog. sect. D*, **54**, 905–921.
24. Battiste, J. L., Li, R. & Woodward, C. (2002). A highly destabilizing mutation, G37A, of the bovine pancreatic trypsin inhibitor retains the average native conformation but greatly increases local flexibility. *Biochemistry*, **41**, 2237–2245.
25. Cierpicki, T. & Otlewski, J. (2000). Determination of a high precision structure of a novel protein, *Linum usitatissimum* trypsin inhibitor (LUTI), using computer-aided assignment of NOESY cross-peaks. *J. Mol. Biol.* **302**, 1179–1192.
26. Güntert, P., Mumenthaler, C. & Herrmann, T. (1998). *Dyana: User's Manual*.
27. Güntert, P., Braun, W. & Wüthrich, K. (1991). Efficient computation of three-dimensional protein structures in solution from nuclear magnetic resonance data using the program DIANA and the supporting programs CALIBA, HABAS and GLOMSA. *J. Mol. Biol.* **217**, 517–530.
28. Nilges, M. (1995). Calculation of protein structures with ambiguous distance restraints. Automated assignment of ambiguous NOE cross-peaks and disulphide connectivities. *J. Mol. Biol.* **245**, 645–660.
29. Wishart, D. S. & Case, D. A. (2001). Use of chemical shifts in macromolecular structure determination. *Methods Enzymol.* **338**, 3–34.
30. Kim, K. S., Tao, F., Fuchs, J., Danishefsky, A. T., Housset, D., Wlodawer, A. & Woodward, C. (1993). Crevice-forming mutants of bovine pancreatic trypsin inhibitor: stability changes and new hydrophobic surface. *Protein Sci.* **2**, 588–596.
31. Andersen, N. H., Neidigh, J. W., Harris, S. M., Lee, G. M., Liu, Z. & Tong, H. (1997). Extracting information from the temperature gradients of polypeptide NH chemical shifts. 1. The importance of conformational averaging. *J. Am. Chem. Soc.* **119**, 8547–8561.
32. Kuroda, Y. & Kim, P. S. (2000). Folding of bovine pancreatic trypsin inhibitor (BPTI) variants in which almost half the residues are alanine. *J. Mol. Biol.* **298**, 493–501.
33. Wells, J. A. (1990). Additivity of mutational effects in proteins. *Biochemistry*, **29**, 8509–8517.
34. Beeser, S. A., Goldenberg, D. P. & Oas, T. G. (1997). Enhanced protein flexibility caused by a destabilizing amino acid replacement in BPTI. *J. Mol. Biol.* **269**, 154–164.
35. Bode, W. & Huber, R. (1992). Natural protein proteinase inhibitors and their interaction with proteinases. *Eur. J. Biochem.* **204**, 433–451.
36. Otlewski, J., Krowarsch, D. & Apostoluk, W. (1999). Protein inhibitors of serine proteinases. *Acta Biochim. Pol.* **46**, 531–565.
37. Apostoluk, W. & Otlewski, J. (1998). Variability of the canonical loop conformations in serine proteinases inhibitors and other proteins. *Proteins: Struct. Funct. Genet.* **32**, 459–474.
38. Braunschweiler, L. & Ernst, R. R. (1983). Coherence transfer by isotropic mixing: application to proton correlation spectroscopy. *J. Magn. Reson.* **53**, 521–528.
39. Bax, A. & Davis, D. G. (1985). MLEV-17 based two-dimensional homonuclear magnetization transfer spectroscopy. *J. Magn. Reson.* **65**, 355–360.
40. Rance, M., Sorensen, O. W., Bodenhausen, G., Wagner, G., Ernst, R. R. & Wuthrich, K. (1983). Improved spectral resolution in COSY ^{1}H NMR spectra of proteins *via* double quantum filtering. *Biochem. Biophys. Res. Commun.* **117**, 479–485.
41. Kumar, A., Ernst, R. R. & Wüthrich, K. (1980). A two-dimensional nuclear Overhauser enhancement (2D NOE) experiment for the elucidation of complete proton–proton cross-relaxation networks in biological macromolecules. *Biochem. Biophys. Res. Commun.* **95**, 1–6.
42. Delaglio, F., Grzesiek, S., Vuister, G. W., Zhu, G., Pfeifer, J. & Bax, A. (1995). NMRPipe: a multidimensional spectral processing system based on UNIX pipes. *J. Biomol. NMR*, **6**, 277–293.
43. Smallcombe, S. H., Patt, S. L. & Keifer, P. A. (1995). WET solvent suppresion and its application to LC NMR and high-resolution NMR spectroscopy. *J. Magn. Reson. A*, **117**, 295–303.
44. Wüthrich, K. (1986). *NMR of Proteins and Nucleic Acids*, Wiley, New York.

45. Baxter, N. J. & Williamson, M. P. (1997). Temperature dependence of 1H chemical shifts in proteins. *J. Biomol. NMR*, **9**, 359–369.
46. Goddard, T. D. & Kneller, D. G. *SPARKY 3*, University of California, San Francisco
47. Delaglio, F., Wu, Z. & Bax, A. (2001). Measurement of homonuclear proton couplings from regular 2D COSY spectra. *J. Magn. Reson.* **149**, 276–281.
48. Güntert, P., Mumenthaler, C. & Wüthrich, K. (1997). Torsion angle dynamics for NMR structure calculation with the new program DYANA. *J. Mol. Biol.* **273**, 283–298.
49. Laskowski, R. A., Rullmannn, J. A., MacArthur, M. W., Kaptein, R. & Thornton, J. M. (1996). AQUA and PROCHECK-NMR: programs for checking the quality of protein structures solved by NMR. *J. Biomol. NMR*, **8**, 477–486.
50. Koradi, R., Billeter, M. & Wüthrich, K. (1996). MOLMOL: a program for display and analysis of macromolecular structures. *J. Mol. Graph.* **14**, 51–55.
51. Koradi, R., Billeter, M. & Wüthrich, K. (1996). MOLMOL: a program for display and analysis of macromolecular structures. *J. Mol. Graph.* **14**, 29–32.

Edited by R. Huber

(Received 10 April 2002; received in revised form 11 June 2002; accepted 14 June 2002)